High Order Compact Schemes in Projection Methods for Incompressible Viscous Flows

Michel Fournié* and Alain Rigal

Institut de Mathématiques de Toulouse, Université de Toulouse et CNRS (UMR 5219), France.

Abstract. Within the projection schemes for the incompressible Navier-Stokes equations (namely "pressure-correction" method), we consider the simplest method (of order one in time) which takes into account the pressure in both steps of the splitting scheme. For this scheme, we construct, analyze and implement a new high order compact spatial approximation on nonstaggered grids. This approach yields a fourth order accuracy in space with an optimal treatment of the boundary conditions (without error on the velocity) which could be extended to more general splitting. We prove the unconditional stability of the associated Cauchy problem via von Neumann analysis. Then we carry out a normal mode analysis so as to obtain more precise results about the behavior of the numerical solutions. Finally we present detailed numerical tests for the Stokes and the Navier-Stokes equations (including the driven cavity benchmark) to illustrate the theoretical results.

AMS subject classifications: 65M06, 76D05

Key words: Incompressible Navier-Stokes, fractional step method, high order compact scheme, boundary conditions.

1   Introduction

For four decades, projection methods have been widely developed for the numerical simulation of unsteady viscous incompressible flows — Navier-Stokes equations with primitive variables: velocity, pressure. Within this class of methods detailed below, the main purpose of this paper is the construction, analysis and implementation of high order compact space approximations on nonstaggered grids.

---

*Corresponding author. *Email addresses:* `michel.fournie@math.univ-toulouse.fr` (M. Fournié), `alain.rigal@math.univ-toulouse.fr` (A. Rigal)

The survey paper of Guermond, Minev and Shen [32] gave recently a rather complete overview of projection methods for incompressible flows. Our approach belongs to the class of "pressure-correction" methods presented in [32] (Part 3). Projection or splitting methods for incompressible flows were independently introduced by Chorin [1] and Temam [2] forty years ago. They carried out the splitting of velocity and pressure for Navier-Stokes equations which yields independent systems of elliptic equations for the velocity and the pressure. These pioneering works [1, 2] have been published simultaneously with the fractional-step (or splitting) methods for multidimensional partial differential equations problems (see Yanenko [35]). However these splittings imply a decoupling of space variables for elliptic or parabolic problems (generalization of ADI methods [30, 31, 38]). For Navier-Stokes equations, due to the specificity of the pressure (non dynamic variable), the projection methods are not relevant of the fractional step methodology.

The Chorin-Temam projection method [1, 2] completely decouples the velocity and the pressure in two steps. The first step is a "dynamic" step, an intermediate velocity field is computed without taking the pressure into account. In the second step, the pressure is obtained from an elliptic problem including the intermediate velocity carry out in the first step. Through this choice of construction, this projection method is of order 1 independently of the approximation order of the time derivative [5].

The next stage in the development of projection methods begins with the paper of Goda [3] in 1979. The main objective, subsequently followed by Kim-Moin [4], Van Kan [25], was the construction of projection methods of order 2. Therefore the Chorin-Temam approach is modified by the introduction of the pressure gradient in the first step. In this paper we use the splitting of Goda [3]; however our construction and analyzes may be extended to other projection methods.

The major feature of this paper is the use of spatial compact approximations of order 4 in the framework of projection methods. The efficiency, the robustness, the easy treatment of boundary conditions prompt many authors [6, 9, 16, 17, 19, 33, 34], to develop compact difference schemes (nine point schemes for 2D problems) for Navier-Stokes equations in vorticity stream function formulation. We also refer to the papers of Ben-Artzi et al. [20, 21] devoted to a compact scheme for Navier-Stokes equations under this formulation using biharmonic operator. The development of approximation methods for the pressure velocity formulation is crucial because their 3D generalization is quite natural. Following previous works on projection methods [10–12, 15, 37], we use the normal mode analysis developed from the pioneering works of Godunov-Riabenkii, Kreiss et al. [7, 29, 36] devoted to hyperbolic problems. Karniadakis, Israeli and Orszag [5], Orszag, Israeli and Deville [23] are the first authors who have applied this analysis to projection methods. The principle of normal mode analysis is the comparison, using Fourier and Laplace transforms, of the solution modes of the differential problem with the solution modes of the semi-discretized problem and those of the numerical approximation. This approach, in simplified situations, allows some precise results about the behavior of the numerical solutions, the influence of the boundary conditions and the presence of numer-

ical boundary layers. Several recent works provide some detailed analyses of projection methods for Navier-Stokes equations where the normal mode analysis is essential: E and Liu [10–12], Johnston and Liu [15], Pyo and Shen [37]. This quite recent paper [37] gives a thorough normal analysis for two second-order projection methods including a comparison of this approach with the energy method. In our paper, the numerical experiments are carried out so as to illustrate the theoretical results given by normal mode analysis with different choices of parameters, like viscosity and discretization steps.

The main stages of this work are as follows. In Section 2, we introduce the splitting method including time approximation. In Section 3, we construct the spatial compact finite difference schemes of order 4 with new optimal computation of the divergence in the intermediate velocity field. In Section 4, we present the von Neumann stability analysis for the associated Cauchy problem using Fourier transform and the normal mode analysis for a "periodic channel" (we consider a 2D rectangle with periodic boundary conditions in one direction). Section 5 is devoted to the presentation of different numerical examples so as to validate the accuracy and stability properties of the approximation scheme. Finally, we apply our algorithm to the benchmark test for driven cavity problem.

2 Semi-discrete incremental pressure-correction scheme (time discretization)

We consider the time-dependent Navier-Stokes equations on a finite time interval $[0,T]$ and in an open, connected, bounded Lipschitz domain $\Omega = (0,1)^2$,

$$
\begin{cases}
\dfrac{\partial \mathbf{u}}{\partial t} - \nu \Delta \mathbf{u} + (\mathbf{u} \cdot \nabla)\mathbf{u} + \nabla p = \mathbf{f}, & \text{on } \Omega \times (0,T), \\
\text{div}(\mathbf{u}) = 0, & \text{on } \Omega \times (0,T), \\
\mathbf{u} = \mathbf{u}_D, & \text{on } \partial\Omega, \\
\mathbf{u}(t=0) = \mathbf{u}_0,
\end{cases}
\tag{2.1}
$$

where $\mathbf{f}$ is a smooth source term and $\mathbf{u}_0 \in H$ with

$$
H = \left\{ \mathbf{v} \in \left[L^2(\Omega) \right]^2; \ \text{div}(\mathbf{v}) = 0; \ \mathbf{v} \cdot n_{|\partial\Omega} = 0 \right\}.
$$

Since the non linear term in the Navier-Stokes equations does not affect the convergence rate of the splitting error [32], we hereafter shall be mainly concerned with the time-dependent Stokes equations written in terms of the primitive variables, namely the velocity $\mathbf{u}$ and the pressure p. We emphasize that all the results stated in this paper are applicable to the full non linear Navier-Stokes equations provided that sufficient regularity on the solution holds. For the numerical tests, the Navier-Stokes problem is considered with an explicit treatment of the non linear term (Adams-Bashforth) that we add to the source term $\mathbf{f}$ so as to obtain a Stokes problem. In the presentation, the generic right hand side will be denoted by $\mathbf{F}$.

We consider the standard incremental pressure-correction scheme which is a time-marching technique composed of two sub-steps (Part 3 in [32]).

The first sub-step gives a provisional velocity $\mathbf{u}^*$ (the pressure is treated explicitly) and takes viscous effects into account. The second sub-step takes incompressibility into account and is usually referred to the projection step

$$\mathbf{u}^{k+1} = P_H \mathbf{u}^*,$$

where P_H is the L^2-orthogonal projector onto H.

In the original non incremental pressure-correction scheme introduced by Chorin and Temam [1,2], the pressure gradient is obviously missing in the first sub-step. Goda [3] is the first author who has added a former value of pressure gradient in the first sub-step so as to increase the accuracy of the projection scheme. This approach was popularized by Van Kan [25]. To approximate the time derivative, we consider the incremental pressure-correction scheme using the Backward Difference Formula (BDF). Let $\Delta_t > 0$ be a time step and set $t^k = k\Delta_t$, for $0 \leq k \leq K = T/\Delta_t$. For any function g, we denote by g^n the approximation of g at the time level n and introduce

$$\phi^{n+1} = p^{n+1} - p^n.$$

We define the first-order scheme (Implicit Euler) $(BDF1)$

$$\begin{cases} \dfrac{\mathbf{u}^* - \mathbf{u}^n}{\Delta_t} - \nu \Delta \mathbf{u}^* = \mathbf{F}^n - \nabla p^n, & \text{on } \Omega, \\ \mathbf{u}^* = \mathbf{u}_D^{n+1}, & \text{on } \partial\Omega, \end{cases} \tag{2.2a}$$

$$\begin{cases} \dfrac{\mathbf{u}^{n+1} - \mathbf{u}^*}{\Delta_t} + \nabla \phi^{n+1} = 0, & \text{on } \Omega, \\ \text{div}(\mathbf{u}^{n+1}) = 0, & \text{on } \Omega, \\ \mathbf{u}^{n+1} \cdot \vec{n} = \mathbf{u}_D^{n+1} \cdot \vec{n}, & \text{on } \partial\Omega. \end{cases} \tag{2.2b}$$

The above algorithm can be generalized to a large class of time-marching algorithms using higher order backward difference formula (see $(BDFq)$ in [32]). For example the second-order scheme (3 time levels) $(BDF2)$ can be formulated by

$$\begin{cases} \dfrac{1}{\Delta_t}\left[\dfrac{3}{2}\mathbf{u}^* - \left(2\mathbf{u}^n - \dfrac{1}{2}\mathbf{u}^{n-1}\right)\right] - \nu \Delta \mathbf{u}^* = \mathbf{F}^n - \nabla p^n, \\ \mathbf{u}^* = \mathbf{u}_D^{n+1}, \quad \text{on } \partial\Omega, \end{cases} \tag{2.3a}$$

$$\begin{cases} \dfrac{3}{2\Delta_t}\left(\mathbf{u}^{n+1} - \mathbf{u}^*\right) + \nabla \phi^{n+1} = 0, & \text{on } \Omega, \\ \text{div}(\mathbf{u}^{n+1}) = 0, & \text{on } \Omega, \\ \mathbf{u}^{n+1} \cdot \vec{n} = \mathbf{u}_D^{n+1} \cdot \vec{n}, & \text{on } \partial\Omega. \end{cases} \tag{2.3b}$$

However, the splitting scheme has an irreducible splitting error of low order in time [25]. Hence, using a higher-order time stepping scheme does not significantly improve the overall accuracy. So, we focus the present work on $(BDF1)$ scheme that allows a thorough analysis of the accuracy and stability. The present approach is also applicable to more general algorithms of higher order in time but for such schemes an overall analysis can not be realized.

3 High-order compact scheme (space discretization)

We choose a regular two-dimensional nonstaggered cartesian grid on $\Omega = (0,1)^2$, with grid spacings Δ_x and Δ_y in x and y direction respectively. We index the nodes with $i = 0, \cdots, N_x + 1$, with respect to x, $j = 0, \cdots, N_y + 1$, for y and the boundaries correspond to $i = 0$, $i = N_x + 1$, $j = 0$, $j = N_y + 1$. For any function g, we denote $g_{i,j}$ the approximation of g at the point indexed by (i,j).

The velocity $\mathbf{u}_{i,j} = (u_{i,j}, v_{i,j})$ is computed for $i = 0, \cdots, N_x + 1$, $j = 0, \cdots, N_y + 1$, and the pressure $p_{i,j}$ is only computed on the interior nodes $i = 1, \cdots, N_x$, $j = 1, \cdots, N_y$.

This choice differs from a nonstaggered grids approach considering the nodes on the boundaries for the pressure that is known to not prevent pressure oscillations [41]. The capability of nonstaggered grids using a local pressure boundary conditions is proved in [18].

We denote δ_{x0} the first-order central difference with respect to x

$$\delta_{x0} g_{i,j} = \frac{g_{i+1,j} - g_{i-1,j}}{2\Delta_x}.$$

The forward and backward operators are denoted δ_{x+} and δ_{x-}, respectively

$$\delta_{x+} g_{i,j} = \frac{g_{i+1,j} - g_{i,j}}{\Delta_x} \quad \text{and} \quad \delta_{x-} g_{i,j} = \frac{g_{i,j} - g_{i-1,j}}{\Delta_x}.$$

The standard second-order central difference is denoted δ_x^2

$$\delta_x^2 g_{i,j} = \delta_{x+} \delta_{x-} g_{i,j} = \frac{g_{i+1,j} - 2g_{i,j} + g_{i-1,j}}{\Delta_x^2}.$$

The difference operators δ_{y0}, δ_{y+}, δ_{y-} and δ_y^2 are similarly defined. Our fourth order scheme is based on the fourth order approximations (see [7,9])

$$\frac{\partial}{\partial x} = \left(1 + \frac{\Delta_x^2}{6}\delta_x^2\right)^{-1}\delta_{x0} + \mathcal{O}(\Delta_x^4), \tag{3.1a}$$

$$\frac{\partial^2}{\partial x^2} = \left(1 + \frac{\Delta_x^2}{12}\delta_x^2\right)^{-1}\delta_x^2 + \mathcal{O}(\Delta_x^4). \tag{3.1b}$$

The approximation (3.1a) can be deduced from the non compact approximation (see [7])

$$\frac{\partial}{\partial x} = \left(1 - \frac{\Delta_x^2}{6}\delta_x^2\right)\delta_{x0} + \mathcal{O}(\Delta_x^4). \tag{3.2}$$

When the reference node is the central node (i,j), we omit the indexes for example $\delta_{x0}g = \delta_{x0}g_{i,j}$.

3.1 Discretization of the first step (for the intermediate velocity $\mathbf{u}^*$)

The classical high order compact scheme can be used for the first step. Using the approximations (3.1a), (3.1b) and replacing $\mathbf{F}^n - \nabla p^n$ by $\tilde{\mathbf{F}}^n$, the first step of $(BDF1)$ scheme (2.2) is written as

$$\frac{\mathbf{u}^* - \mathbf{u}^n}{\Delta_t} - \nu\left[\left(1 + \frac{\Delta_x^2}{12}\delta_x^2\right)^{-1}\delta_x^2\mathbf{u}^* + \left(1 + \frac{\Delta_y^2}{12}\delta_y^2\right)^{-1}\delta_y^2\mathbf{u}^*\right] = \tilde{\mathbf{F}}^n. \tag{3.3}$$

We multiply both sides of (3.3) by

$$A = \left(1 + \frac{\Delta_x^2}{12}\delta_x^2\right)\left(1 + \frac{\Delta_y^2}{12}\delta_y^2\right) = 1 + \frac{\Delta_x^2}{12}\delta_x^2 + \frac{\Delta_y^2}{12}\delta_y^2 + \mathcal{O}(\Delta_x^2\Delta_y^2)$$

(neglecting the terms of order higher than 4) and obtain

$$A\left(\frac{\mathbf{u}_{i,j}^* - \mathbf{u}_{i,j}^n}{\Delta_t}\right) - \nu\left[\left(1 + \frac{\Delta_y^2}{12}\delta_y^2\right)\delta_x^2 + \left(1 + \frac{\Delta_x^2}{12}\delta_x^2\right)\delta_y^2\right]\mathbf{u}^* = A\tilde{\mathbf{F}}^n.$$

Let us define

$$B = \left(1 + \frac{\Delta_y^2}{12}\delta_y^2\right)\delta_x^2 + \left(1 + \frac{\Delta_x^2}{12}\delta_x^2\right)\delta_y^2.$$

Then $\mathbf{u}^*$ is given by

$$\left(\frac{A}{\Delta_t} - \nu B\right)\mathbf{u}^* = A\left(\tilde{\mathbf{F}}^n + \frac{\mathbf{u}^n}{\Delta_t}\right). \tag{3.4}$$

The stencils associated with the operators A and B are compact with the shape

$$\begin{array}{ccc} \bullet_{i-1,j+1} & \bullet_{i,j+1} & \bullet_{i+1,j+1} \\ \bullet_{i-1,j} & \bullet_{i,j} & \bullet_{i+1,j} \\ \bullet_{i-1,j-1} & \bullet_{i,j-1} & \bullet_{i+1,j-1} \end{array}$$

In matrix form, the coefficients of A and B are respectively given by

$$\begin{bmatrix} & \frac{1}{12} & \\ \frac{1}{12} & \frac{2}{3} & \frac{1}{12} \\ & \frac{1}{12} & \end{bmatrix} \quad \text{and} \quad \begin{bmatrix} \frac{1}{12\Delta_y^2} + \frac{1}{12\Delta_x^2} & \frac{5}{6\Delta_y^2} - \frac{1}{6\Delta_x^2} & \frac{1}{12\Delta_y^2} + \frac{1}{12\Delta_x^2} \\ -\frac{1}{6\Delta_y^2} + \frac{5}{6\Delta_x^2} & -\frac{5}{3\Delta_y^2} - \frac{5}{3\Delta_x^2} & -\frac{1}{6\Delta_y^2} + \frac{5}{6\Delta_x^2} \\ \frac{1}{12\Delta_y^2} + \frac{1}{12\Delta_x^2} & \frac{5}{6\Delta_y^2} - \frac{1}{6\Delta_x^2} & \frac{1}{12\Delta_y^2} + \frac{1}{12\Delta_x^2} \end{bmatrix}.$$

Remark 3.1. The compactness property is crucial for a direct and accurate treatment of the boundary conditions (see below). The right hand side of (3.4) contains ∇p^n (in the generic right hand side $\tilde{\mathbf{F}}^n$) and must be carefully computed. For the sake of simplicity, in the next section, we carry out an explicit non compact approximation of order 4 given by

$$\nabla_x p^n = \left(1 - \frac{\Delta_x^2}{6}\delta_x^2\right)\delta_{x0}p^n \quad \text{and} \quad \nabla_y p^n = \left(1 - \frac{\Delta_y^2}{6}\delta_y^2\right)\delta_{y0}p^n.$$

3.2 Discretization of the second sub-step (for the pressure p^{n+1} via Φ^{n+1})

Using the divergence equation in $(BDF1)$ (2.2), we can characterize the pressure by the following Poisson-Neumann system

$$\begin{cases} \Delta\phi^{n+1} = \dfrac{1}{\Delta_t}\text{div}(\mathbf{u}^*), & \text{on } \Omega, \\[2mm] \dfrac{\partial\phi^{n+1}}{\partial n} = 0, & \text{on } \partial\Omega. \end{cases} \tag{3.5}$$

We refer to the literature for pressure boundary conditions which are not consistent boundary conditions [13]. For the sake of clarity, we considered the homogeneous Neumann boundary condition. A natural extension of the present work can be made for other type of boundary conditions.

In this step, the main difficulties consist in the computation of $\text{div}(\mathbf{u}^*)$ in the right hand side of (3.5) and in the treatment of the boundary conditions. We now present a new computation process using high-order compact discretization. Using classical fourth-order discretization based on (3.1b) (and similar formula in y-direction), the problem (3.5) is approximated by

$$\left(1 + \frac{\Delta_x^2}{12}\delta_x^2\right)^{-1}\delta_x^2\phi^{n+1} + \left(1 + \frac{\Delta_y^2}{12}\delta_y^2\right)^{-1}\delta_y^2\phi^{n+1} = \frac{1}{\Delta_t}\text{div}(\mathbf{u}^*).$$

With the same computations used to obtain (3.4) we have

$$\left(1 + \frac{\Delta_y^2}{12}\delta_y^2\right)\delta_x^2\phi^{n+1} + \left(1 + \frac{\Delta_x^2}{12}\delta_x^2\right)\delta_y^2\phi^{n+1} = \left(1 + \frac{\Delta_x^2}{12}\delta_x^2\right)\left(1 + \frac{\Delta_y^2}{12}\delta_y^2\right)\frac{1}{\Delta_t}\text{div}(\mathbf{u}^*).$$

This scheme can be written with the compact operators A and B defined in (3.4)

$$B\phi^{n+1} = A\frac{1}{\Delta_t}\text{div}(\mathbf{u}^*). \tag{3.6}$$

We need a specific treatment to compute the right hand side of (3.6) at the order 4 and to preserve the compactness property. First, we can express $\text{div}(\mathbf{u}^*)$ using the non compact approximation (3.2)

$$\text{div}(\mathbf{u}^*) = \left(\left(1 - \frac{\Delta_x^2}{6}\delta_x^2\right)\delta_{x0}u^* + \left(1 - \frac{\Delta_y^2}{6}\delta_y^2\right)\delta_{y0}v^*\right). \tag{3.7}$$

Applying operator A to (3.7) and neglecting High Order Terms (HOT: terms of order higher than 4), we obtain

$$A\text{div}(\mathbf{u}^*) = \delta_{x0}u^* + \delta_{y0}v^* + \frac{\Delta_x^2}{12}\left(\delta_x^2\delta_{y0}v^* - \delta_x^2\delta_{x0}u^*\right) + \frac{\Delta_y^2}{12}\left(\delta_y^2\delta_{x0}u^* - \delta_y^2\delta_{y0}v^*\right) + HOT.$$

We can rewrite this expression to reveal $(\delta_x^2 u^* + \delta_y^2 u^*)$ and $(\delta_x^2 v^* + \delta_y^2 v^*)$,

$$\begin{aligned}
A\text{div}(\mathbf{u}^*) = {}& \delta_{x0}u^* + \delta_{y0}v^* + \left(\frac{\Delta_x^2}{12} + \frac{\Delta_y^2}{12}\right)\delta_y^2\delta_{x0}u^* + \left(\frac{\Delta_x^2}{12} + \frac{\Delta_y^2}{12}\right)\delta_x^2\delta_{y0}v^* \\
& - \frac{\Delta_x^2}{12}\delta_{x0}\underbrace{\left(\delta_x^2 u^* + \delta_y^2 u^*\right)}_{\approx \Delta u^*} - \frac{\Delta_y^2}{12}\delta_{y0}\underbrace{\left(\delta_x^2 v^* + \delta_y^2 v^*\right)}_{\approx \Delta v^*} + HOT.
\end{aligned}$$

Moreover from the first sub step in $(BDF1)$ scheme (2.2) we can explicitly compute Δu^* and Δv^*

$$\Delta\mathbf{u}^* = \frac{1}{\nu}\left(\frac{\mathbf{u}^* - \mathbf{u}^n}{\Delta_t} - \tilde{\mathbf{F}}^n\right). \tag{3.8}$$

So, the computation of ϕ is given by

$$\begin{aligned}
& \left(\delta_x^2 + \delta_y^2 + \left(\frac{\Delta_x^2}{12} + \frac{\Delta_y^2}{12}\right)\delta_y^2\delta_x^2\right)\phi^{n+1} \\
& = \frac{1}{\Delta_t}\left[-\frac{\Delta_x^2}{12\nu}\delta_{x0}\left(\frac{u^* - u^n}{\Delta_t} - \tilde{F}_1^n\right) - \frac{\Delta_y^2}{12\nu}\delta_{y0}\left(\frac{v^* - v^n}{\Delta_t} - \tilde{F}_2^n\right) + \delta_{x0}u^* \right. \\
& \left. \quad + \delta_{y0}v^* + \left(\frac{\Delta_x^2}{12} + \frac{\Delta_y^2}{12}\right)\delta_y^2\delta_{x0}u^* + \left(\frac{\Delta_x^2}{12} + \frac{\Delta_y^2}{12}\right)\delta_x^2\delta_{y0}v^*\right].
\end{aligned} \tag{3.9}$$

In (3.9), the unknown ϕ^{n+1} is only computed on the interior nodes ($i = 1, \cdots, N_x$ and $j = 1, \cdots, N_y$) contrary to $\mathbf{u}$ and $\mathbf{u}^*$ defined in the whole domain. Then the computation of the right hand side of (3.9) is straightforward without introduction of numerical error. The situation is different for the left hand side where the finite difference formula requires ϕ^{n+1} on the boundaries ($i = 0$, $N_x + 1$ and $j = 0$, $N_y + 1$). To overcome this difficulty, we take the homogeneous Neumann boundary condition on ϕ into account to deduce the following approximations of order 2, 3 and 4 [9] for the boundary $y = 0$

$$\phi_{0,j} = \phi_{1,j} + \mathcal{O}(\Delta_x^2), \tag{3.10a}$$

$$\phi_{0,j} = \frac{4}{3}\phi_{1,j} - \frac{1}{3}\phi_{2,j} + \mathcal{O}(\Delta_x^3), \tag{3.10b}$$

$$\phi_{0,j} = \frac{18}{11}\phi_{1,j} - \frac{9}{11}\phi_{2,j} + \frac{2}{11}\phi_{3,j} + \mathcal{O}(\Delta_x^4). \tag{3.10c}$$

From numerical experiments with the three boundary formulas (3.10a), (3.10b), (3.10c), we do not observe significant differences. So we retain the simplest scheme (3.10a) which

preserves the compactness character of the discretization. We suggest that the error introduced by (3.10a) is smaller than the error arising from the choice of the homogeneous Neumann boundary condition in (3.5).

Remark 3.2. We refer to the paper of Gustafsson [26] to justify that the global convergence rate is not destroyed by lower order numerical boundary conditions.

In conclusion, the determination of ϕ on the compact stencil is given by (3.9) using (3.10a).

3.3 Discretization of the second sub-step (for the velocity $\mathbf{u}^{n+1}$)

We consider the equation

$$\frac{1}{\Delta_t}(\mathbf{u}^{n+1} - \mathbf{u}^*) + \nabla \phi^{n+1} = 0.$$

For the first component of velocity u, we use the difference operator (3.1a) to approximate the first derivative and applying $(1 + \Delta_x^2 \delta_x^2 / 6)$, we obtain

$$\left(1 + \frac{\Delta_x^2}{6} \delta_x^2\right) \left(\frac{1}{\Delta_t}(u^{n+1} - u^*)\right) + \delta_{x0} \phi^{n+1} = 0.$$

We denote M_x the operator $(1 + \Delta_x^2 \delta_x^2 / 6)$, and obtain u by solving

$$M_x u^{n+1} = M_x u^* - \Delta_t \delta_{x0} \phi^{n+1}, \tag{3.11}$$

where M_x is compact and its coefficients are given by

$$\begin{bmatrix} 0 & 0 & 0 \\ \frac{1}{6} & \frac{2}{3} & \frac{1}{6} \\ 0 & 0 & 0 \end{bmatrix}.$$

The second component of velocity v is similarly obtained

$$M_y v^{n+1} = M_y v^* - \Delta_t \delta_{y0} \phi^{n+1}, \tag{3.12}$$

where M_y is compact and its coefficients are given by

$$\begin{bmatrix} 0 & \frac{1}{6} & 0 \\ 0 & \frac{2}{3} & 0 \\ 0 & \frac{1}{6} & 0 \end{bmatrix}.$$

Due to the compactness of the operators, no specific treatment of the boundaries is necessary for the velocity and (3.10c) is used for the pressure.

4 Analysis of the projection schemes

In the first paragraph, we consider the linearized problem and prove the unconditional stability in von Neumann sense. In the second paragraph, we demonstrate the stability of the scheme using Godunov-Ryabenki (normal mode) analysis. To simplify the presentation we fix $\Delta_x = \Delta_y = h$.

4.1 von Neumann analysis

To analyze the stability of the $(BDF1)$ scheme (2.2), we consider the homogeneous Cauchy problem and use Fourier transform by replacing $u_{i,j}$, $v_{i,j}$, $p_{i,j}$, by $\hat{u}e^{I(iz_1+jz_2)}$, $\hat{v}e^{I(iz_1+jz_2)}$, $\hat{p}e^{I(iz_1+jz_2)}$, respectively with (z_1,z_2) in the range $[-\pi,\pi]$ and I the imaginary pure unit.

Firstly, we eliminate the auxiliary intermediate field (u^*,v^*) and write the difference scheme as a one-step recurrence in $\mathbb{R}^3$, where $(u^{n+1},v^{n+1},p^{n+1})$ depends on (u^n,v^n,p^n). We denote

$$A_x = \left(1 + \frac{h^2}{6}\delta_x^2\right), \quad B_x = \left(1 + \frac{h^2}{12}\delta_x^2\right),$$

and analogously A_y and B_y in the y-direction.

From (3.4), (3.11) and (3.12) we have

$$
\begin{cases}
u^* = \dfrac{1}{2}\left(\nu\Delta_t A_x(B_x\delta_y^2 + B_y\delta_x^2)\right)^{-1}\left((A_x+A_y)(A_x u^{n+1} + \Delta_t\delta_{x0}p^{n+1} - A_x u^n)\right), \\[2mm]
v^* = \dfrac{1}{2}\left(\nu\Delta_t A_y(B_x\delta_y^2 + B_y\delta_x^2)\right)^{-1}\left((A_x+A_y)(A_y v^{n+1} + \Delta_t\delta_{y0}p^{n+1} - A_y v^n)\right),
\end{cases}
$$

and we deduce with (3.9)

$$
(B_y\delta_x^2 + B_x\delta_y^2)(p^{n+1} - p^n)
$$
$$
= \frac{1}{12}\left(\nu\Delta_t A_x(B_x\delta_y^2 + B_y\delta_x^2)A_y\right)^{-1}\left(-h^2 A_y B_x\delta_y^2 + A_y(6A_y{}^2 + 6A_y A_x - h^2 B_y\delta_x^2)\right)\delta_{x0}{}^2 p^{n+1}
$$
$$
+ \frac{1}{12}\left(\nu\Delta_t{}^2(B_x\delta_y^2 + B_y\delta_x^2)\right)^{-1}\left(-h^2 B_x\delta_y^2 - h^2 B_y\delta_x^2 + 6A_y A_x + 6A_y{}^2\right)\delta_{x0}(u^{n+1} - u^n)
$$
$$
+ \frac{1}{12}\left(\nu\Delta_t(B_x\delta_y^2 + B_y\delta_x^2)A_y\right)^{-1}\left(-h^2 B_x\delta_y^2 - h^2 B_y\delta_x^2 + 6A_x{}^2 + 6A_y A_x\right)\delta_{y0}{}^2 p^{n+1}
$$
$$
+ \frac{1}{12}\left(\nu\Delta_t{}^2(B_x\delta_y^2 + B_y\delta_x^2)\right)^{-1}\left(-h^2 B_x\delta_y^2 - h^2 B_y\delta_x^2 + 6A_x{}^2 + 6A_y A_x\right)\delta_{y0}(v^{n+1} - v^n).
$$

Finally, from (3.11) and (3.12), we have

$$
\begin{cases}
A_x u^{n+1} = \dfrac{1}{2}\left(\nu\Delta_t(B_x\delta_y^2 + B_y\delta_x^2)\right)^{-1}\left((A_x+A_y)(A_x u^{n+1} + \Delta_t\delta_{x0}p^{n+1} - A_x u^n)\right) \\[2mm]
\qquad\qquad - \Delta_t\delta_{x0}(p^{n+1} - p^n), \\[2mm]
A_y v^{n+1} = \dfrac{1}{2}\left(\nu\Delta_t(B_x\delta_y^2 + B_y\delta_x^2)\right)^{-1}\left((A_x+A_y)(A_y v^{n+1} + \Delta_t\delta_{y0}p^{n+1} - A_x u^n)\right) \\[2mm]
\qquad\qquad - \Delta_t\delta_{y0}(p^{n+1} - p^n).
\end{cases}
\tag{4.1}
$$

Considering $(BDF1)$ scheme (2.2) for $W^n = (u^n, v^n, p^n)^T$, we have

$$M_1 W^{n+1} = M_2 W^n,$$

where the entries of the (3×3) matrix M_1 are given by

$$
\begin{cases}
(M_1)_{1,1} = -\left(\Delta_t^2 \nu (B_x \delta_y^2 + B_y \delta_x^2)\right)^{-1} (-h^2 B_x \delta_y^2 - h^2 B_y \delta_x^2 + 6A_y A_x + 6A_y{}^2)\delta_{x0}, \\
(M_1)_{1,2} = -\left(\Delta_t^2 \nu (B_x \delta_y^2 + B_y \delta_x^2)\right)^{-1} (-h^2 B_x \delta_y^2 - h^2 B_y \delta_x^2 + 6A_x{}^2 + 6A_y A_x)\delta_{y0}, \\
(M_1)_{1,3} = -\left(A_x \Delta_t \nu (B_x \delta_y^2 + B_y \delta_x^2)\right)^{-1} (-h^2 B_x \delta_y^2 - h^2 B_y \delta_x^2 + 6A_y A_x + 6A_y{}^2)\delta_{x0}{}^2 \\
\qquad\quad - (\Delta_t A_y \nu (B_x \delta_y^2 + B_y \delta_x^2))^{-1} (-h^2 B_x \delta_y^2 - h^2 B_y \delta_x^2 + 6A_x{}^2 + 6A_y A_x)\delta_{y0}{}^2 \\
\qquad\quad + 12(B_x \delta_y^2 + B_y \delta_x^2), \\
(M_1)_{2,1} = \left(\nu \Delta_t (B_x \delta_y^2 + B_y \delta_x^2)\right)^{-1} A_x (-A_x - A_y + 2\nu \Delta_t B_x \delta_y^2 + 2\nu \Delta_t B_y \delta_x^2), \\
(M_1)_{2,2} = 0, \\
(M_1)_{2,3} = \left(\nu (B_x \delta_y^2 + B_y \delta_x^2)\right)^{-1} (-A_x - A_y + 2\nu \Delta_t B_x \delta_y^2 + 2\nu \Delta_t B_y \delta_x^2)\delta_{x0}, \\
(M_1)_{3,1} = 0, \\
(M_1)_{3,2} = \left(\nu \Delta_t (B_x \delta_y^2 + B_y \delta_x^2)\right)^{-1} A_y (-A_x - A_y + 2\nu \Delta_t B_x \delta_y^2 + 2\nu \Delta_t B_y \delta_x^2), \\
(M_1)_{3,3} = \left(\nu (B_x \delta_y^2 + B_y \delta_x^2)\right)^{-1} (-A_x - A_y + 2\nu \Delta_t B_x \delta_y^2 + 2\nu \Delta_t B_y \delta_x^2)\delta_{y0},
\end{cases}
\tag{4.2}
$$

and the entries of the (3×3) matrix M_2 are given by

$$
\begin{cases}
(M_2)_{1,1} = (M_1)_{1,1}, \quad (M_2)_{1,2} = (M_1)_{1,2}, \\
(M_2)_{1,3} = 12(B_x \delta_y^2 + B_y \delta_x^2), \\
(M_2)_{2,1} = -\left(\nu \Delta_t (B_x \delta_y^2 + B_y \delta_x^2)\right)^{-1} (A_x + A_y) A_x, \\
(M_2)_{2,2} = 0, \quad (M_2)_{2,3} = 2\Delta_t \delta_{x0}, \quad (M_2)_{3,1} = 0, \\
(M_2)_{3,2} = -\left(\nu \Delta_t (B_x \delta_y^2 + B_y \delta_x^2)\right)^{-1} A_y (A_x + A_y), \quad (M_2)_{3,3} = 2\Delta_t \delta_{y0}.
\end{cases}
\tag{4.3}
$$

So we define a matrix $M = M_1^{-1} M_2$ which satisfies $W^{n+1} = MW^n$ and we use 2D Fourier transform defined above. We get $\widehat{W}^{n+1} = \widehat{M}\widehat{W}^n$ where $\widehat{M} = G(z_1, z_2)$ is the (3×3) amplification matrix of the scheme. $\widehat{M}$ is obtained and simplified using formal calculus tools.

The von Neumann stability is based on the eigenvalues of the amplification matrix. The scheme is stable when the moduli of these eigenvalues are less than or equal to 1 (strictly less than 1 for multiple eigenvalues-Theorem 4.2.1 in [7]).

Theorem 4.1. *The difference scheme $(BDF1)$ (2.2) (Eqs. (3.4), (3.9), (3.11) and (3.12)) is unconditionally stable in the von Neumann sense.*

Proof. For all $(z_1, z_2) \in [-\pi, \pi] - \{(0,0)\}$, let us define a, b, A and B by

$$a = \cos^2 \frac{z_1}{2}, \quad b = \cos^2 \frac{z_2}{2}, \tag{4.4a}$$

$$A = 4 - a - b - 2ab$$

$$= \frac{1}{4}[10 - 4\cos z_1 - 4\cos z_2 - \cos(z_1 + z_2) - \cos(z_1 - z_2)], \tag{4.4b}$$

$$B = 1 + a + b. \tag{4.4c}$$

These terms verify $0 \le a \le 1, 0 \le b \le 1, B > 0$ and $A > 0$ for $(a,b) \ne (1,1)$.

By formal computations, we express the third order characteristic polynomial in function of the mesh ratio $r = \nu \Delta_t / h^2$ under the form $[x - B/(4Ar+B)]p(r)$ where

$$p(r) = a_2(r)x^2 + a_1(r)x + a_0, \tag{4.5}$$

with

$$a_0 = 6(a-b)^2 A + 4(1-a)^2(1-b)^2 B, \tag{4.6a}$$

$$a_1(r) = -4(2a+1)(2b+1)A^2 r - 2a_0, \tag{4.6b}$$

$$a_2(r) = (2a+1)(2b+1)A(4Ar+B). \tag{4.6c}$$

The particular case, $z_1 = 0$, $z_2 = 0$ must be considered separately. In this case, we have one eigenvalue of the amplification matrix $\widehat{M}$ equal to 1 and two others equal to 0.

For $z_1 \ne 0, z_2 \ne 0$, we have one eigenvalue given by

$$vp_1 = \frac{B}{4Ar+B}. \tag{4.7}$$

The eigenvalue vp_1 verifies $0 < vp_1 < 1$, and other eigenvalues are solutions of the second degree polynomial equation (4.5). From (4.6a)-(4.6c), it is clear that $a_2(r) > 0$, $a_1(r) < 0$, $a_0 > 0$, when $(a,b) \ne (1,1)$.

The quantity $a_2(r)$ is an increasing function of $r > 0$, so

$$a_2(r) - a_0 > a_2(0) - a_0 = p_1, \tag{4.8}$$

with

$$p_1 = 27abA + (1-a)(1-b)[3(a+b)A + 3(a+b-2ab)B] > 0, \tag{4.9}$$

because $a + b - 2ab = [2 - \cos(z_1 - z_2) - \cos(z_1 + z_2)]/4$ is strictly positive. The product of the moduli of both roots, equal to $a_0/a_2(r)$, is thus less than 1.

The discriminant Δ of equation (4.5) may be written

$$\Delta = 16(2a+1)^2(2b+1)^2 A^4 r^2 - 4a_0 p_1, \tag{4.10}$$

so, for given a and b, there exists $r_0 > 0$, such that $\Delta \le 0$, for $0 < r \le r_0$ and $\Delta > 0$, for $r > r_0$. In the first case, both roots have the same modulus, less than 1 like their product. When

$r > r_0$, Eq. (4.5) has two positive roots and one of them is less than 1 because the product of the two roots is less than 1. It is now easy to check that

$$p(1) = a_2(0) - a_0 = p_1 > 0, \tag{4.11}$$

so 1 is outside the roots interval and both roots also lie inside the unit disk. □

4.2 Normal mode analysis

In this section we demonstrate the stability and fourth-order accuracy of the new ($BDF1$) scheme (2.2) using Godunov-Ryabenki (normal mode) analysis. We consider the unsteady 2D Stokes equations on $[-1,1] \times (0,2\pi) \times (0,T)$ given by

$$\begin{cases} \dfrac{\partial \mathbf{u}}{\partial t} - \nu \Delta \mathbf{u} + \nabla p = 0, \\ \operatorname{div}(\mathbf{u}) = 0, \end{cases} \tag{4.12}$$

with periodic boundary conditions in y and no-slip boundary condition $\mathbf{u}=0$, for $x=-1,1$. We assume solutions of the form

$$u(x,y,t) = e^{iky} u(x,t), \quad v(x,y,t) = e^{iky} v(x,t), \quad p(x,y,t) = e^{iky} p(x,t). \tag{4.13}$$

For simplicity we use the same notations for u,v and p in both sides of these relations. Then the solutions of (4.12) are reduced to a family of 1D problems, indexed by $k \in \mathbb{Z}$, given by

$$\begin{cases} \dfrac{\partial u}{\partial t} + \dfrac{\partial p}{\partial x} - \nu \dfrac{\partial^2 u}{\partial x^2} + \nu k^2 u = 0, \\ \dfrac{\partial v}{\partial t} + ikp - \nu \dfrac{\partial^2 v}{\partial x^2} + \nu k^2 v = 0, \\ \dfrac{\partial u}{\partial x} + ikv = 0, \end{cases} \tag{4.14}$$

with the boundary conditions $u(\pm 1,t) = v(\pm 1,t) = 0$.

The normal mode solutions of (4.14) take the form

$$u(x,t) = e^{\sigma t} u(x), \quad v(x,t) = e^{\sigma t} v(x), \quad p(x,t) = e^{\sigma t} p(x). \tag{4.15}$$

By plugging (4.15) into (4.14), we obtain

$$\begin{cases} \sigma u + \dfrac{\partial p}{\partial x} - \nu \dfrac{\partial^2 u}{\partial x^2} + \nu k^2 u = 0, \\ \sigma v + ikp - \nu \dfrac{\partial^2 v}{\partial x^2} + \nu k^2 v = 0, \\ \dfrac{\partial u}{\partial x} + ikv = 0, \end{cases} \tag{4.16}$$

with boundary conditions

$$u(\pm 1) = v(\pm 1) = 0. \tag{4.17}$$

There are two families of solutions, symmetric and antisymmetric (odd and even). The analysis of each solution is essentially the same and we focus on the former. The odd solutions of (4.16) are given by

$$\begin{cases} u = A\cosh(kx) + B\cos(\mu x), \\ v = \dfrac{i}{k}(Ak\sinh(kx) - B\mu\sin(\mu x)), \\ p = -\sigma\dfrac{A}{k}\sinh(kx), \end{cases} \tag{4.18}$$

where

$$\sigma = -\nu(\mu^2 + k^2). \tag{4.19}$$

It then follows that $\sigma < 0$ in (4.15) and as expected the solutions of (4.12) decay in time.

In order to satisfy the boundary conditions $u(\pm 1) = v(\pm 1) = 0$, constants A and B in (4.18) must verify

$$\begin{cases} A\cosh(k) + B\cos(\mu) = 0, \\ -Ak\sinh(k) + B\mu\sin(\mu) = 0. \end{cases} \tag{4.20}$$

From (4.20), we deduce a compatibility condition. In the interval $(-\pi/2 + l\pi, \pi/2 + l\pi)$, $l = 0, \pm 1, \pm 2, \cdots$, there is a unique real solution μ which satisfies

$$\mu\tan(\mu) + k\tanh(k) = 0. \tag{4.21}$$

We can express the symmetric solutions

$$\begin{cases} u(x) = \cos(\mu x) - \dfrac{\cos(\mu)\cosh(kx)}{\cosh(k)}, \\ v(x) = \dfrac{-i\sin(\mu x)\mu}{k} - \dfrac{i\cos(\mu)\sinh(kx)}{\cosh(k)}, \\ p(x) = \dfrac{\sigma\cos(\mu)\sinh(kx)}{k\cosh(k)}. \end{cases} \tag{4.22}$$

Finally, from (4.21) and (4.22), we remark that the incompressibility condition is satisfied.

We now carry out analogous calculations for the compact finite difference scheme ($BDF1$) (2.2) (Eqs. (3.4), (3.9), (3.11) and (3.12)). Using (4.13), we obtain

$$\begin{cases} \dfrac{u^{*n+1} - u^n}{\Delta_t} - \dfrac{\partial^2 u^{*n+1}}{\partial x^2} + \dfrac{\partial p^n}{\partial x} + k^2 u^{*n+1} = 0, & \text{on } \Omega, \\ \dfrac{v^{*n+1} - v^n}{\Delta_t} - \dfrac{\partial^2 v^{*n+1}}{\partial x^2} + ikp^n + k^2 v^{*n+1} = 0, & \text{on } \Omega, \\ \mathbf{u}^{*n+1}(\pm 1, t) = 0, \end{cases} \tag{4.23a}$$

$$
\begin{cases}
\dfrac{u^{n+1}-u^{*n+1}}{\Delta_t}+\dfrac{\partial p^{n+1}}{\partial x}-\dfrac{\partial p^n}{\partial x}=0, & \text{on } \Omega, \\[2mm]
\dfrac{v^{n+1}-v^{*n+1}}{\Delta_t}+ik(p^{n+1}-p^n)=0, & \text{on } \Omega, \\[2mm]
\dfrac{\partial u^{n+1}}{\partial x}+ikv^{n+1}=0, & \text{on } \Omega, \\[2mm]
\mathbf{u}^{n+1}\cdot\vec{n}(\pm1,t)=0.
\end{cases}
\tag{4.23b}
$$

For the semi-discrete problem (4.23), we assume normal mode solutions of the form

$$
u^n=\kappa^n u(x), \qquad v^n=\kappa^n v(x), \qquad p^n=\kappa^n p(x),
\tag{4.24a}
$$
$$
u^{*n+1}=\kappa^{n+1}u^*(x), \qquad v^{*n+1}=\kappa^{n+1}v^*(x).
\tag{4.24b}
$$

By plugging (4.24) into (4.23), we obtain

$$
\begin{cases}
\dfrac{\kappa u^*-u}{\Delta_t}-\kappa\dfrac{\partial^2 u^*}{\partial x^2}+\dfrac{\partial p}{\partial x}+k^2\kappa u^*=0, & \text{on } \Omega, \\[2mm]
\dfrac{\kappa v^*-v}{\Delta_t}-\kappa\dfrac{\partial^2 v^*}{\partial x^2}+ikp+k^2\kappa v^*=0, & \text{on } \Omega, \\[2mm]
\mathbf{u}^*(\pm1,t)=0,
\end{cases}
\tag{4.25a}
$$

$$
\begin{cases}
\kappa\dfrac{u-u^*}{\Delta_t}+\kappa\dfrac{\partial p}{\partial x}-\dfrac{\partial p}{\partial x}=0, & \text{on } \Omega, \\[2mm]
\kappa\dfrac{v-v^*}{\Delta_t}+ikp(\kappa-1)=0, & \text{on } \Omega, \\[2mm]
\dfrac{\partial u}{\partial x}+ikv=0, & \text{on } \Omega, \\[2mm]
\mathbf{u}\cdot\vec{n}(\pm1,t)=0.
\end{cases}
\tag{4.25b}
$$

The set of the resulting equations can be solved and we get two families of solutions, even and odd. The odd solutions are given by

$$
u(x)=-\frac{\kappa\Delta_t Ak\cosh(kx)}{-1+\kappa}-\frac{kD\cos(\mu x)}{\mu},
\tag{4.26a}
$$
$$
v(x)=\frac{-i\Delta_t kA\kappa\sinh(kx)}{-1+\kappa}+iD\sin(\mu x),
\tag{4.26b}
$$
$$
u^*(x)=-\frac{(2\kappa-1)\Delta_t Ak\cosh(kx)}{(-1+\kappa)\kappa}+\frac{(-1+\kappa)\lambda C\Delta_t\cos(\lambda x)}{\kappa}-\frac{kD\cos(\mu x)}{\mu},
\tag{4.26c}
$$
$$
v^*(x)=\frac{-i(2\kappa-1)kA\Delta_t\sinh(kx)}{(-1+\kappa)\kappa}+\frac{i(-1+\kappa)k\Delta_t C\sin(\lambda x)}{\kappa}+iD\sin(\mu x),
\tag{4.26d}
$$
$$
p(x)=A\sinh(kx)+C\sin(\lambda x),
\tag{4.26e}
$$

where

$$
\lambda^2=\frac{\kappa}{\nu(1-\kappa)\Delta_t}-k^2, \qquad \mu^2=-k+\frac{1-\kappa}{\nu\kappa\Delta_t}.
\tag{4.27}
$$

In order to satisfy the boundary conditions $u^*(\pm 1) = 0$, $v^*(\pm 1) = 0$, $u(\pm 1) = 0$ constants A, C and D in (4.26) must verify

$$-\frac{(2\kappa-1)\Delta_t Ak\cosh(k)}{(-1+\kappa)\kappa}+\frac{(-1+\kappa)\lambda C\Delta_t\cos(\lambda)}{\kappa}-\frac{kD\cos(\mu)}{\mu}=0, \tag{4.28a}$$

$$-\frac{(2\kappa-1)\Delta_t Ak\sinh(k)}{(-1+\kappa)\kappa}+\frac{(-1+\kappa)k\Delta_t\sin(\lambda)C}{\kappa}+D\sin(\mu)=0, \tag{4.28b}$$

$$-\frac{\kappa\Delta_t Ak\cosh(k)}{-1+\kappa}-\frac{kD\cos(\mu)}{\mu}=0. \tag{4.28c}$$

From (4.28), we deduce a compatibility condition. In the interval $(-\pi/2+l\pi, \pi/2+l\pi)$, $l=0,\pm 1,\pm 2,\cdots$, there is a unique real solution μ which satisfies

$$k\frac{(2\kappa-1)}{\kappa^2}\tanh(k)+k^2\frac{(-1+\kappa)^2}{\kappa^2\lambda}\tan(\lambda)+\tan(\mu)\mu=0. \tag{4.29}$$

Therefore, the values of A, C and D are given by

$$A=\frac{\mu\cos(\mu)(-1+\kappa)}{k\Delta_t\cosh(k)\mu\kappa}, \quad C=-\frac{k\mu\cos(\mu)(-1+\kappa)}{k\lambda\cos(\lambda)\kappa\Delta_t\mu}, \quad D=-\frac{\mu}{k}.$$

So we deduce the solutions of the semi-discretized system (4.25)

$$u(x)=-\frac{\cos(\mu)\cosh(kx)}{\cosh(k)}+\cos(\mu x), \tag{4.30a}$$

$$v(x)=-\frac{i\cos(\mu)\sinh(kx)}{\cosh(k)}-\frac{i\sin(\mu x)\mu}{k}, \tag{4.30b}$$

$$u^*(x)=-\frac{\cos(\mu)(2\kappa-1)\cosh(kx)}{\kappa^2\cosh(k)}-\frac{\cos(\mu)(-1+\kappa)^2\cos(\lambda x)}{\cos(\lambda)\kappa^2}+\cos(\mu x), \tag{4.30c}$$

$$v^*(x)=-\frac{i\cos(\mu)(2\kappa-1)\sinh(kx)}{\kappa^2\cosh(k)}-\frac{i\cos(\mu)k(-1+\kappa)^2\sin(\lambda x)}{\lambda\cos(\lambda)\kappa^2}-\frac{i\sin(\mu x)\mu}{k}, \tag{4.30d}$$

$$p(x)=\frac{\cos(\mu)(-1+\kappa)\sinh(kx)}{\Delta_t\cosh(k)k\kappa}-\frac{\cos(\mu)(-1+\kappa)\sin(\lambda x)}{\lambda\cos(\lambda)\kappa\Delta_t}. \tag{4.30e}$$

It is clear from (4.30) that the numerical scheme has a couple of new modes not shared by the original problem (4.12). We see that there is a fundamental change of character in the numerical profile of p. These spurious numerical modes represented by λ defined in (4.27) are introduced by the projection procedure and do not appear in the velocity. By identification of the growth rate κ in (4.13) and the growth rate $e^{\sigma\Delta_t}$ in (4.24a), we can deduce the accuracy in time of the projection method. Indeed,

$$\frac{\kappa-1}{\kappa\Delta_t}=\sigma+\mathcal{O}(\Delta_t).$$

This implies that the accuracy is in Δ_t, the order of the finite difference approximation introduced by the time discretization.

We can observe from the form of the spurious numerical modes and the definition of λ that the error introduced in the pressure must be controlled to keep λ real ($\lambda^2 = \kappa/\nu(1-\kappa)\Delta_t - k^2 \geq 0$). This constraint supposes that $\nu\Delta_t$ is sufficiently small in comparison with modes k. This remark is confirmed by numerical tests (see section below). A related analysis is carried out by Strikwerda and Lee [8] who used a normal mode analysis in the half-plane and showed that the pressure approximation can be first-order accurate at most.

Now we consider the finite difference discretization of (2.2) using (3.4), (3.9), (3.11) and (3.12). Plugging (4.30) into these discrete equations, we compute the corresponding errors denoted by $\mathrm{Err}^{u^*}_{(3.4)}$, $\mathrm{Err}^{v^*}_{(3.4)}$ for the first and second components of the intermediate field in (3.4), $\mathrm{Err}^{u}_{(3.11)}$, $\mathrm{Err}^{v}_{(3.12)}$ for the first and second components of the velocity in (3.11), (3.12) and $\mathrm{Err}^{p}_{(3.9)}$ for the pressure in (3.9). We obtain

$$
\begin{cases}
\mathrm{Err}^{u^*}_{(3.4)} = 72e^{iky}k\kappa\nu\Delta_t{}^2(-1+k)\cos(\mu x)+\mathcal{O}(h^4), \\
\mathrm{Err}^{v^*}_{(3.4)} = -72ie^{iky}\nu\kappa\Delta_t{}^2\mu(-1+k)\sin(\mu x)+\mathcal{O}(h^4), \\
\mathrm{Err}^{u}_{(3.11)} = \mathcal{O}(h^4), \quad \mathrm{Err}^{v}_{(3.12)} = \mathcal{O}(h^4), \quad \mathrm{Err}^{p}_{(3.9)} = \mathcal{O}(h^4).
\end{cases}
\tag{4.31}
$$

We observe a second-order error in time in the computation of u^* and v^* only. Moreover, the above expressions in (4.31) confirm the fourth order of the spatial approximation. The global accuracy of the algorithm is governed by the splitting error (of order 1 in our case). This error can be improved with minor modifications (see [32]).

5 Numerical examples

In order to validate the proposed scheme and test its robustness, we apply it to different Stokes and Navier-Stokes 2D problems. The computations are made on various grid sizes and time steps, and for different values of the viscosity. We report the maximum absolute errors for the velocity and the pressure on the grids and compute some rates of convergence. All results are linked with theoretical arguments.

5.1 Stokes problem

Test 5.1. Stationary polynomial example for Stokes problem.

We consider $\Omega = (0,1) \times (0,1)$ and consider the exact solution (u,v,p) given by

$$
\begin{cases}
u(x,y,t) = x^2(1-x)^2(2y-6y^2+4y^3), \\
v(x,y,t) = -y^2(1-y)^2(2x-6x^2+4x^3), \\
p(x,y,t) = x^2y^2(2x-3)(2y-3).
\end{cases}
\tag{5.1}
$$

The source term **f** in (2.1) is deduced from the exact solution.

Remark 5.1. This example does not introduce non physical boundary condition. Indeed, our scheme enforces Neumann boundary condition $\partial p/\partial n = 0$ which is not generally the right one. Then we do not introduce numerical boundary layer which would limit the accuracy of the scheme.

In the following, $N = 1/\Delta_x = 1/\Delta_y$ represents the number of grid points in both directions and $N_k = 1/\Delta_t$ represents the number of iterations necessary to arrive at the final time $T_f = 1$. The solution does not depend on time, however it is computed using our algorithm which is a time marching process. So the method can be interpreted as a fixed point algorithm. Here, the iteration in time (in relation with N_k) must be considered as an iteration index independent of time.

In Tables 1 and 2 we consider the Stokes problem with ν equal to 1 and 10^{-2} respectively and report the errors on (u,v,p) in maximum norm after 100 iterations ($\Delta_t = 10^{-2}$). In Figs. 1 and 2, we plot the $Log(\text{error})$ versus $Log(\Delta_x)$ to study the slope of the curves associated to Tables 1 and 2, respectively.

Table 1: Errors for $\nu = 1$ after 100 iterations.

N	err_∞^u	err_∞^v	err_∞^p
20	0.1958292E-06	0.1958292E-06	0.1252270E-05
30	0.3872679E-07	0.3872679E-07	0.2844922E-06
40	0.1227335E-07	0.1227335E-07	0.9602300E-07
50	0.5036730E-08	0.5036730E-08	0.4079812E-07
60	0.2430611E-08	0.2430611E-08	0.2013498E-07
70	0.1312240E-08	0.1312240E-08	0.1104018E-07
80	0.7692046E-09	0.7692046E-09	0.6547615E-08
90	0.4801650E-09	0.4801650E-09	0.4124670E-08
100	0.3149938E-09	0.3149937E-09	0.2724832E-08

Table 2: Errors for $\nu = 10^{-2}$ after 100 iterations.

N	err_∞^u	err_∞^v	err_∞^p
20	0.8462582E-07	0.8462582E-07	0.9762751E-08
30	0.1683172E-07	0.1683172E-07	0.2223235E-08
40	0.5316980E-08	0.5316980E-08	0.7525865E-09
50	0.2187092E-08	0.2187092E-08	0.3202063E-09
60	0.1054144E-08	0.1054144E-08	0.1583109E-09
70	0.5693178E-09	0.5693178E-09	0.8701462E-10
80	0.3339215E-09	0.3339215E-09	0.5172651E-10
90	0.2083148E-09	0.2083148E-09	0.3265532E-10
100	0.1367918E-09	0.1367918E-09	0.2161893E-10

Remark 5.2. We observe the same behavior for different choices of the number of iterations N_k, which emphasizes the time independence.
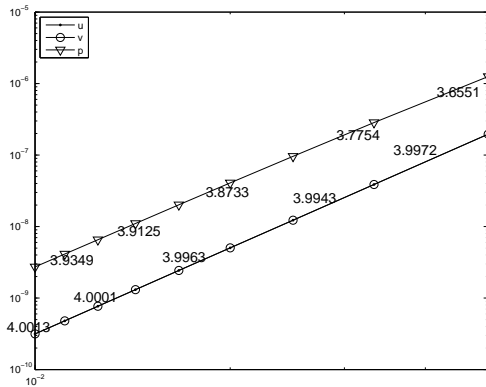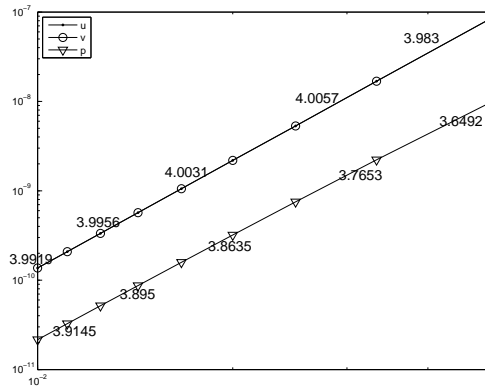
Figure 1: Rates of convergence for Table 1.

Figure 2: Rates of convergence for Table 2.

This stationary numerical example allows to verify the fourth order accuracy of the high order compact approximation. The rates of convergence are very close to 4 for both values of ν. Reducing the value of ν, the absolute errors decrease in particular for the error on the pressure (the decreasing factor is approximately equal to ν). The error on the pressure is larger than the error on the velocity for $\nu = 1$ and we observe a switch between these errors for $\nu = 10^{-2}$. We refer to the following test for justifications.

Test 5.2. Non stationary example for Stokes problem.

We consider the flow decayed by viscosity problem [6, 20] governed by the Stokes equations in $\Omega = (0,1) \times (0,1)$, which has analytical solutions given by

$$\begin{cases} u(x,y,t) = -\cos(\pi x)\sin(\pi y)e^{-2t\nu}, \\ v(x,y,t) = \sin(\pi x)\cos(\pi y)e^{-2t\nu}, \\ p(x,y,t) = -\dfrac{1}{4}\left[\cos(2\pi x) + \cos(2\pi y)\right]e^{-4t\nu}. \end{cases} \tag{5.2}$$

For this problem, the solution is computed at the final time $T_f = 1$. Note that the time accuracy of the splitting scheme is intrinsically of first order (independently of the time discretization scheme-see the Section 4.2 on normal mode analysis and [5]), so a high order accuracy is difficult to observe.

In Tables 3 and 4, the errors are given for $\nu = 1$ using different time steps $\Delta_t = 10^{-2}$ and $\Delta_t = 10^{-3}$ respectively. The associated rate of convergence plots are shown in Figs. 3 and 4. We observe that the error on the pressure is dominant in comparison with the errors on the velocity components. When Δ_t is not sufficiently small (Table 3), a numerical locking on the pressure is observed (the error on the pressure slightly increases for $N \geq 50$). This phenomenon disappears when we take a smaller value of Δ_t (Table 4).

Remark 5.3. Numerical locking is already observed in paper [32] and the inconsistency between theoretical and numerical results is explained. In particular, the importance of the norms used for error analysis is outlined with non uniform error estimates.

Table 3: $\nu = 1$, $\Delta_t = 10^{-2}$ and $T_f = 1$.

Δ_x	err_∞^u	err_∞^v	err_∞^p
0.5000000E-01	0.1233524E-03	0.1311406E-03	0.7547192E-02
0.3333333E-01	0.6997886E-04	0.7630907E-04	0.3360876E-02
0.2500000E-01	0.4186219E-04	0.4679139E-04	0.1812012E-02
0.2000000E-01	0.2591338E-04	0.2995322E-04	0.1287058E-02
0.1666667E-01	0.1606394E-04	0.1938024E-04	0.1806931E-02
0.1428571E-01	0.9608855E-05	0.1241132E-04	0.2318810E-02
0.1250000E-01	0.7186720E-05	0.7960057E-05	0.2662619E-02
0.1111111E-01	0.6502817E-05	0.7103729E-05	0.2903055E-02
0.1000000E-01	0.6066820E-05	0.7098557E-05	0.3076859E-02

Table 4: $\nu = 1$, $\Delta_t = 10^{-3}$ and $T_f = 1$.

| Δ_x	err_∞^u	err_∞^v	err_∞^p
0.5000000E-01	0.1288364E-03	0.1296244E-03	0.9609371E-02
0.3333333E-01	0.7780175E-04	0.7847844E-04	0.5607374E-02
0.2500000E-01	0.5091399E-04	0.5146454E-04	0.3703372E-02
0.2000000E-01	0.3559771E-04	0.3606961E-04	0.2652050E-02
0.1666667E-01	0.2622014E-04	0.2662426E-04	0.1997495E-02
0.1428571E-01	0.2005423E-04	0.2041232E-04	0.1563452E-02
0.1250000E-01	0.1582012E-04	0.1613757E-04	0.1259447E-02
0.1111111E-01	0.1277771E-04	0.1306553E-04	0.1037530E-02
0.1000000E-01	0.1053014E-04	0.1079103E-04	0.8701147E-03
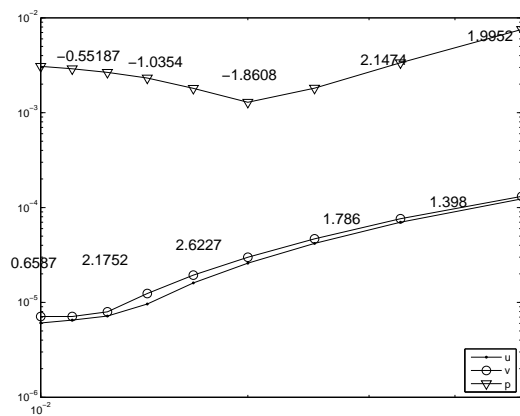
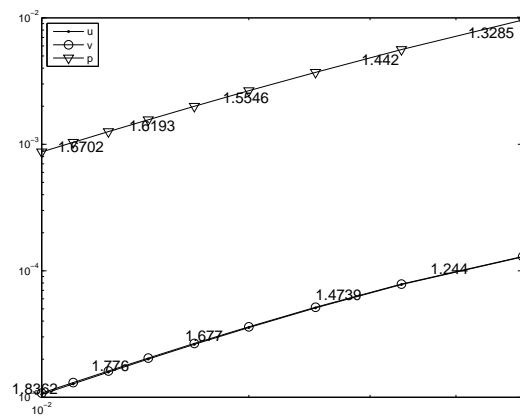Figure 3: Rates of convergence for Table 3.

Figure 4: Rates of convergence for Table 4.

Numerical results for smaller values of viscosity are given in Tables 5 and 6 for $\nu = 10^{-2}$ and $\nu = 10^{-3}$ respectively. Corresponding convergence graphs are given in Figs. 5 and 6. We observe better results when ν decreases (which is a good behavior for many

Table 5: $\nu = 10^{-2}$, $\Delta_t = 10^{-3}$ and $T_f = 1$.

Δ_x	err_∞^u	err_∞^v	err_∞^p
0.5000000E-01	0.4244778E-03	0.4244431E-03	0.4086144E-03
0.3333333E-01	0.2736903E-03	0.2737142E-03	0.2413999E-03
0.2500000E-01	0.1846338E-03	0.1846609E-03	0.1598767E-03
0.2000000E-01	0.1322363E-03	0.1322616E-03	0.1150902E-03
0.1666667E-01	0.9875961E-04	0.9878186E-04	0.8605229E-04
0.1428571E-01	0.7652394E-04	0.7654402E-04	0.6795741E-04
0.1250000E-01	0.6089793E-04	0.6091582E-04	0.5436766E-04
0.1111111E-01	0.4962310E-04	0.4963944E-04	0.4519655E-04
0.1000000E-01	0.4116901E-04	0.4118383E-04	0.3776019E-04

Table 6: $\nu = 10^{-3}$, $\Delta_t = 10^{-3}$ and $T_f = 1$.

| Δ_x	err_∞^u	err_∞^v	err_∞^p
0.5000000E-01	0.1890485E-03	0.1890308E-03	0.4252715E-04
0.3333333E-01	0.1380316E-03	0.1380280E-03	0.3132902E-04
0.2500000E-01	0.1080305E-03	0.1080295E-03	0.2205604E-04
0.2000000E-01	0.8577757E-04	0.8577730E-04	0.1611181E-04
0.1666667E-01	0.6896707E-04	0.6896702E-04	0.1218756E-04
0.1428571E-01	0.5636801E-04	0.5636806E-04	0.9606198E-05
0.1250000E-01	0.4673419E-04	0.4673426E-04	0.7707441E-05
0.1111111E-01	0.3930466E-04	0.3930475E-04	0.6383898E-05
0.1000000E-01	0.3345764E-04	0.3345772E-04	0.5328079E-05
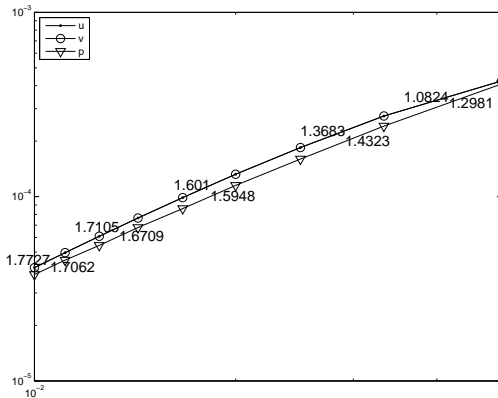
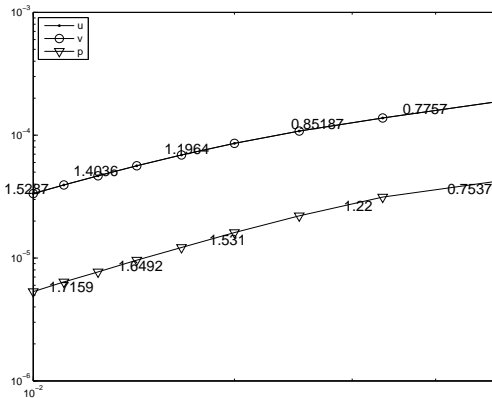Figure 5: Rates of convergence for Table 5.

Figure 6: Rates of convergence for Table 6.

applications-large values of the Reynolds number). In particular the accuracy on the pressure becomes better than the accuracy on the velocity. This point can be justified by the normal mode analysis. Indeed, the spurious numerical modes are governed by λ defined in (4.27) which must be a real value. When $\nu\Delta_t$ decreases, λ increases and the

additional term in the pressure term p in (4.30) decreases. Moreover the influence of the boundary condition for the pressure is less important for weakly viscous flows.

In the above tests, the theoretical rates of convergence are not observed. The structure of the global approximation error of our algorithm is very intricate. Therefore, many numerical tests cannot clearly show an accuracy of order 4. We suggest that this limitation is governed by the first order in time of the splitting (and time discretization) which prevents to observe high order rates. Indeed, when Δ_x decreases (with few points) the fourth-order discretization give us rapidly a good accuracy smaller than the error in time. However, high order can be recovered considering Δ_t and Δ_x dependent. In Tables 7, 8 (Figs. 7, 8), we impose that the discrete Reynolds number $Re_h = \nu\Delta_t/\Delta_x^2$ is fixed and equal to 1. For this choice the scheme presents a very good behavior and reveals its capability to capture an accurate solution with few discretization points and few iteration steps. These tests outline the stability and robustness of the algorithm.

Table 7: $\nu = 10^{-2}$, $\nu\Delta_t/\Delta_x^2 = 1$ and $T_f = 1$.

Δ_x	err_∞^u	err_∞^v	err_∞^p
0.5000000E-01	0.1688531E-02	0.1691965E-02	0.2497973E-02
0.3333333E-01	0.2528387E-03	0.2546877E-03	0.4522883E-03
0.2500000E-01	0.5175519E-04	0.5245221E-04	0.8670854E-04

Table 8: $\nu = 10^{-3}$, $\nu\Delta_t/\Delta_x^2 = 1$ and $T_f = 1$.

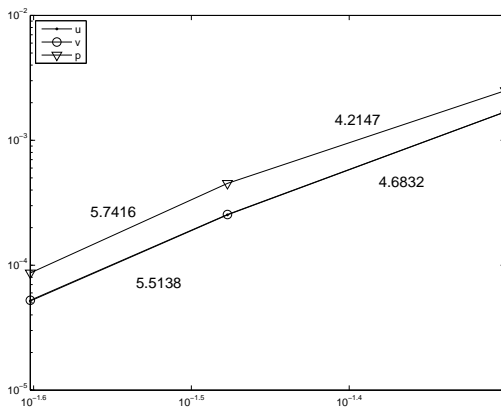| Δ_x	err_∞^u	err_∞^v	err_∞^p
0.1666667E-01	0.1966207E-03	0.1963517E-03	0.5089191E-04
0.1111111E-01	0.2370202E-04	0.2361196E-04	0.6071143E-05
0.8333333E-02	0.2934769E-05	0.2983764E-05	0.9637596E-06

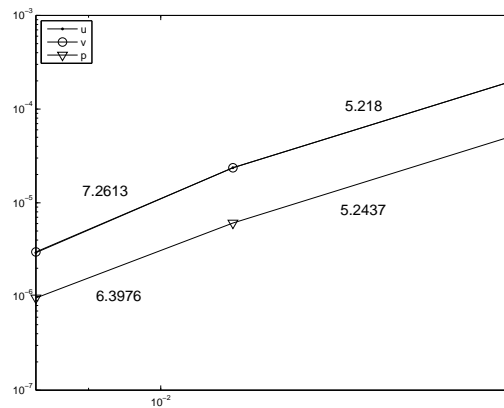Figure 7: Rates of convergence for Table 7.

Figure 8: Rates of convergence for Table 8.

Test 5.3. Navier-Stokes problem-Comparison with driven cavity benchmark.

For Navier-Stokes problem, the same test problems (5.1) and (5.2) give similar behavior, so we present results for the classical driven cavity problem where high order schemes in space are recommended, in particular for high Reynolds number simulations [40]. So we solve the model problem for $\nu = 10^{-3}$ with $\Delta_x = \Delta_y = 1/128$ ($N = 128$) and we compare our results with those obtained by Ghia et al. [39] as the benchmark solutions. In [39] the steady Navier-Stokes equations in the stream function-vorticity formulation is used. This approach, however, does not reveal the time evolution of the flow after the lid is set in motion. At $t = 0$ the lid velocity u is instantaneously set from zero to one, thereby slowly setting in motion the fluid initially at rest. The formation of the large primary eddy as well as that of the first counter-rotating secondary eddy in the lower right corner can be observed rather well. The counter-rotating eddy in the lower left corner, however, needs considerably longer time interval to develop.
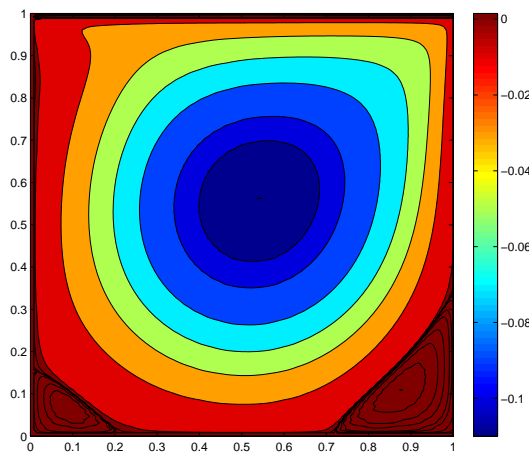

Figure 9: Streamlines for $\nu = 10^{-3}$ with $\Delta_x = \Delta_y = 1/128$.

The streamlines contours for this test are presented in Fig. 9. The computation of the streamlines is a post-process task and is performed using simple finite difference approximation. More precisely, we consider $\partial\psi/\partial x = -v$, with $\psi(x=0) = 0$. For all $j = 0, \cdots, N$, $\psi_{0,j} = 0$, so using first order approximation we deduce $\psi_{1,j} = -\Delta_x v_{0,j} + \psi_{0,j} = 0$ and using second order approximation we compute $\psi_{i,j} = -2\Delta_x v_{i-1,j} + \psi_{i-2,j}$, for $i = 2, \cdots, N$. This figure is comparable with the well known figure obtained in [39] with the same position of the center in $[0.53125, 0.5625]$. The value of ψ at this point is equal to -0.110046 and is very closed to the benchmark solution of Ghia et al. [39] where $\psi = -0.117929$. This difference can be explained by the post-process which is less accurate than a computation of ψ by solving the Navier-Stokes problem in Streamline-Vorticity formulation.

Figs. 10 and 11 show the velocity profiles for u along the vertical lines and v along the horizontal lines passing through the geometric center of the cavity. The values given in [39] are reported in the figures and used to validate our results.
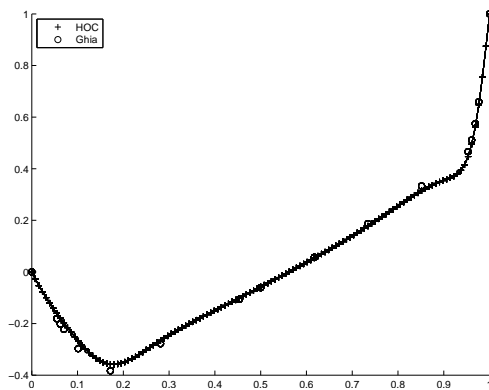
Figure 10: Vertical profile for u.
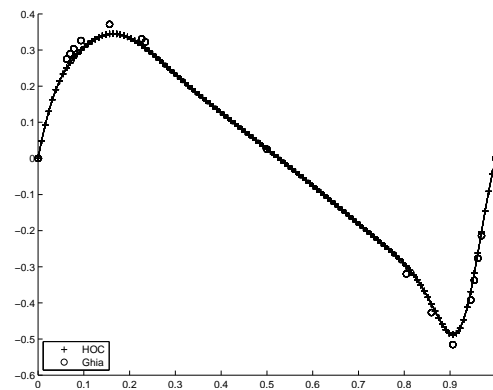
Figure 11: Horizontal profile for v.

6 Conclusions

In this paper, we present a detailed construction of a new compact scheme of order 4 for projection methods on nonstaggered grids. We employed tensorized central 3 points difference operators which allows an efficient implementation. The treatment of the boundary condition is optimal for the velocity and among different choices we retain an approximation of the pressure which preserves the compactness of the scheme. A rigorous analysis of von Neumann type and a thorough normal mode analysis have been carried out. The main advantage of the normal mode analysis is that it reveals the particular error structures, such as spurious boundary layer or spurious highly oscillatory terms and their explicit dependence on dynamic viscosity ν. Hence, the projection-type schemes are particularly suitable for high Reynolds number flows. We observed that supplementary terms introduced by high order terms do not deteriorate the structure of the solution and allow to obtain unconditional stability. Although we use a first order projection method, the accuracy and the rates of convergence of numerical results are very satisfactory for a reasonable range of values of the viscosity ν (1 to 10^{-3}). We emphasize that our scheme presents a very good stability and robustness for a wide field of values of the parameters : time and space steps, viscosity. Moreover, the computed solution for the driven cavity may be favorably compared with the benchmark solutions.

References

[1] A. J. Chorin, The Numerical Solution of the Navier-Stokes Equations for an Incompressible Fluid, AEC Research and Developpement REPORT, NYO-1480-82, New York University, New York, 1967.

[2] R. Temam, Navier-Stokes Equations, Theory and Numerical Analysis, North-Holland, Amsterdanm, 1979.

[3] K. Goda, A multistep technique with implicit difference scheme for calculating two or three dimentional cavity flows, J. Comput. Phys., 30 (1979), 76–95.

[4] J. Kim, and P. Moin, Application of a fractional step method to imcompressible Navier-Stokes equations, J. Comput. Phys., 30 (1985), 308–323.

[5] G. E. Karniadakis, M. Israeli, and S. A. Orszag, High-order splitting methods for the incompressible Navier-Stokes equations, J. Comput. Phys., 97 (1991), 414–443.

[6] J. C. Kalita, and S. Sen, The (9,5) HOC formulation for the transient Navier-Stokes equations in primitive variable, Int. J. Numer. Meth. Fluids., 55 (2007), 387–406.

[7] J. C. Strikwerda, Finite Difference Schemes and Partial Differential Equations, Second edition, Society for Industrial and Applied Mathematics (SIAM), Philadelphia, PA, 2004.

[8] J. C. Strikwerda, and Y. S. Lee, The accuracy of the fractional step method, SIAM J. Numer. Anal., 37(1) (1999), 37–47.

[9] J. C. Strikwerda, High-order-accurate schemes for incompressible viscous flow, Int. J. Numer. Methods. Fluids., 24(7) (1997), 715–734.

[10] W.-N. E, and J.-G. Liu, Projection method, I: convergence and numerical boundary layers, SIAM J. Numer. Anal., 32(4) (1995), 1017–1057.

[11] W.-N. E, and J.-G. Liu, Projection method, II: Godunov-Ryabenki analysis, SIAM J. Numer. Anal., 33(4) (1996), 1597–1621.

[12] W.-N. E, and J.-G. Liu, Projection method, III: spatial discretization on the staggered grid, Math. Comput., 71(237) (2002), 27–47.

[13] D. L. Brown, C. Ricardo, and M. L. Minion, Accurate projection methods for the incompressible Navier-Stokes equations, J. Comput. Phys., 168(2) (2001), 464–499.

[14] G. Em. Karniadakis, M. Israeli, and S. A. Orszag, High-order splitting methods for the incompressible Navier-Stokes equations, J. Comput. Phys., 97(2) (1991), 414–443.

[15] H. Johnston, and J.-G. Liu, Accurate, stable and efficient Navier-Stokes solvers based on explicit treatment of the pressure term, J. Comput. Phys., 199(1) (2004), 221–259.

[16] C. Wang, J.-G. Liu, and H. Johnston, Analysis of a fourth order finite difference method for the incompressible Boussinesq equations, Numer. Math., 97(3) (2004), 555–594.

[17] J.-G. Liu, C. Wang, and H. Johnston, A fourth order scheme for incompressible Boussinesq equations, J. Sci. Comput., 18(2) (2003), 253–285.

[18] H. Johnston, and J.-G. Liu, Finite difference schemes for incompressible flow based on local pressure boundary conditions, J. Comput. Phys., 180(1) (2002), 120–154.

[19] W.-N. E, and J.-G. Liu, Essentially compact schemes for unsteady viscous incompressible flows, J. Comput. Phys., 126(1) (1996), 122–138.

[20] M. Ben-Artzi, J.-P. Croisille, D. Fishelov, and S. Trachtenberg, A pure-compact scheme for the streamfunction formulation of Navier-Stokes equations, J. Comput. Phys., 205 (2005), 640–664.

[21] M. Ben-Artzi, J.-P. Croisille, and D. Fishelov, Convergence of a compact scheme for the pure streamfunction formulation of the unsteady Navier-Stokes system, SIAM J. Numer. Anal., 44(5) (2006), 1997–2024.

[22] R. Temam, Navier-Stokes Equations, Theory and Numerical Analysis, Revised edition, with an appendix by F. Thomasset, Studies in Mathematics and its Applications, 2, North-Holland Publishing Co., Amsterdam-New York, 1979.

[23] S. A. Orszag, M. Israeli, and M. O. Deville, Boundary conditions for incompressible flows, J. Sci. Comput., 1 (1986), 75–111.

[24] J. B. Bell, P. Colella, and H. M. Glaz, A second-order projection method for the incompressible Navier-Stokes equations, J. Comput. Phys., 85(2) (1989), 257–283.

[25] J. Van Kan, A second-order accurate pressure-correction scheme for viscous incompressible flow, SIAM J. Sci. Statist. Comput., 7(3) (1986), 870–891.

[26] B. Gustafsson, The convergence rate for difference approximations to general mixed initial-boundary value problems, SIAM J. Numer. Anal., 18(2) (1981), 179–190.

[27] B. Gustafsson, H.-O. Kreiss, and A. Sundström, Stability theory of difference approximations for mixed initial-boundary value problems, II, Math. Comput., 26 (1972), 649–686.

[28] S. Osher, Stability of difference equations of dissipative type for mixed initial-boundary value problems, I, Math. Comput., 23 (1969), 335–340.

[29] H. O. Kreiss, and J. Lorenz, Initial-Boundary Value Problems and the Navier-Stokes Equations, Pure and Applied Mathematics, 136, Academic Press, Inc., Boston, MA, 1989.

[30] R. M. Beam, and R. F. Warming, Alternating direction implicit methods for parabolic equations with a mixed derivative, SIAM J. Sci. Statist. Comput., 1(1) (1980), 131–159.

[31] A. R. Mitchell, and G. Fairweather, Improved forms of the alternating direction methods of Douglas, Peaceman, and Rachford for solving parabolic and elliptic equations, Numer. Math., 6 (1964), 285–292.

[32] J. L. Guermond, P. Minev, and J. Shen, An overview of projection methods for incompressible flows, Comput. Methods. Appl. Mech. Engrg., 195(44-47) (2006), 6011–6045.

[33] W. D. Henshaw, A fourth-order accurate method for the incompressible Navier-Stokes equations on overlapping grids, J. Comput. Phys., 113(1) (1994), 13–25.

[34] W. D. Henshaw, H.-O, Kreiss, and L. G. M. Reyna, A fourth-order-accurate difference approximation for the incompressible Navier-Stokes equations, Comput. Fluids., 23(4) (1994), 575–593.

[35] N. N. Yanenko, The Method of Fractional Steps, The Solution of Problems of Mathematical Physics in Several Variables, Translated from the Russian by T. Cheron. English translation edited by M. Holt, Springer-Verlag, New York-Heidelberg, 1971.

[36] B. Gustafsson, H.-O. Kreiss, and J. Oliger, Time Dependent Problems and Difference Methods, Wiley-Interscience, 1996.

[37] J. H. Pyo, and J. Shen, Normal mode analysis of second-order projection methods for incompressible flows, Discrete. Contin. Dyn. Syst. Ser. B., 5(3) (2005), 817–840.

[38] D. W. Peaceman, and H. H. Rachford, The numerical solution of parabolic and elliptic differential equations, J. Soc. Ind. Appl. Math., 3 (1955), 28–41.

[39] U. Ghia, K. N. Ghia, and C. T. Shin, High-re solutions for imcompressible flow using the Navier-Stokes equations and a multigrid method, J. Comput. Phys., 48 (1987), 387–411.

[40] H. Nishida, and H. Satofuka, Higher-order solutions of square driven cavity flow using a variable-order multi-grid method, Int. J. Numer. Methods. Eng., 34 (1992), 637–653.

[41] S. W. Armfield, Finite difference solutions of the Navier-Stokes equations on staggered and non-staggered grids, Comput. Fluids., 20 (1991), 1–17.